Response of Southern Hemisphere western boundary current regions to future zonally symmetric and asymmetric atmospheric changes

Rishav Goyal[1,2,*], Matthew H England[1,2,3], Martin Jucker[1,2] and Alex Sen Gupta[1,2,3]

1. Climate Change Research Centre, University of New South Wales, NSW, 2052 Australia

2. ARC Centre of Excellence for Climate Extremes, University of New South Wales, NSW, Australia

3. Australian Centre for Excellence in Antarctic Science (ACEAS), University of New South Wales, NSW, Australia

[*]*Corresponding author: rishav.goyal@unsw.edu.au*

Key points

1. Strong warming in the subtropical western boundary current extension regions is projected in the future
2. Zonally asymmetric atmospheric changes can explain >30% of future warming in the south Australia region, driven by ocean circulation changes
3. Understanding historical and future ocean changes requires the use of regionally varying and not simply zonally symmetric wind forcing

Abstract

Subtropical Western Boundary Currents (WBCs) are often associated with hotspots of global warming, with certain WBC extension regions warming 3-4 times faster than the global mean. In the Southern Hemisphere strong warming over the WBC extensions has been observed over the last few decades, with enhanced warming projected into the future. This amplified warming has primarily been linked to poleward intensification of the mid-latitude westerly winds in the Southern Hemisphere. Changes in these winds are often thought of as being zonally symmetric, however, recent studies show that they contain strong zonal asymmetries in certain ocean basins. The importance of these zonal asymmetries for the Southern Ocean has not yet been investigated. In this study, we use an ocean-sea-ice model forced by prescribed atmospheric fields to quantify the contribution of projected zonally asymmetric atmospheric changes in generating future ocean warming and circulation changes in the subtropical WBC regions of the Southern Hemisphere. We find that the projected zonally asymmetric component of atmospheric change can explain more than 30% (>2°C) of the SST warming found in the Tasman Sea and southern Australia region and a sizeable fraction of warming in the Agulhas Current region. These changes in SST in both the Indian and Pacific Ocean basins are found to be primarily driven by changes in the large-scale subtropical ocean gyres, which in turn can largely be explained by changes in the surface wind stress patterns.

Plain Language Summary

Strong ocean currents are found on the western side of the ocean basins, which flow from the tropics toward the poles in both hemispheres. These western boundary currents have shown strong changes in the last few decades, which have resulted in amplified ocean warming in the poleward extensions of these boundary currents; these changes are projected to amplify further in the future. In the Southern Hemisphere, recent changes in the western boundary currents are thought to have been primarily driven by changes in the surface westerly winds that encircle Antarctica. These westerly winds are generally considered to be changing uniformly in all three ocean basins, however, recent studies have shown that there are strong regional variations both historically and in future projections. Here we find that regional asymmetries in wind projections can account for about 30% of the projected warming in the Tasman Sea and the southern Australia region and a sizeable fraction of warming in the Agulhas Current region. This amplified warming in the Indian and the Pacific Ocean basins is primarily driven by changes in ocean circulation.

1. Introduction

Subtropical western boundary currents (WBCs) are narrow, fast-flowing currents on the western side of the ocean basins which transport warm tropical waters to the mid-latitudes and form the western limb of the subtropical ocean gyres. WBCs are primarily driven by basin-scale surface winds and are generally present in the upper 1000-1500 meters of the ocean. They play a crucial role in the redistribution of heat (Cronin et al., 2010; Ganachaud & Wunsch, 2003), pollutants (Rossi et al., 2013, Eriksen et al., 2013), biogeochemical tracers (Williams & Follows, 2003) and marine larvae (Everett et al., 2017). Subtropical WBCs also release large amounts of heat and moisture along their paths affecting the atmospheric circulation, mid-latitude storms as well as ocean carbon uptake (Kwon et al., 2010; Minobe et al., 2008; Takahashi et al., 2009).

In the Southern Hemisphere, there are three major subtropical WBCs, the East Australia Current (EAC) in the Pacific, the Agulhas Current in the Indian Ocean and the Brazil Current in the Atlantic Ocean. Poleward extensions of these major subtropical WBCs in the Southern Hemisphere are also the hotspots of global warming in the ocean and these regions have shown amplified surface warming as compared to the global averaged Sea Surface Temperature (SST) warming rate over the last few decades (Wu et al., 2012). For instance, the EAC extension region in the South Pacific Ocean basin has been warming at 3-4 times the global averaged SST warming rate over the last few decades (Oliver & Holbrook, 2014).

This amplified warming has been linked to the intensification of the WBC poleward extensions (Wu et al., 2012) and has significant impacts on the ocean biogeochemistry and marine ecology because of the intrusion of warm lower latitude waters in the relatively cooler mid-

latitude waters (Dubois et al., 2016). In the South Pacific, strong warming over the EAC extension region was reported by early studies using in-situ Conductivity, Temperature and Depth (CTD) and Expendable Bathythermograph (XBT) measurements (e.g., Ridgway et al., 2008; Roemmich et al., 2007) and was associated with a strengthening of the EAC extension (Ridgway, 2007). In the Atlantic Ocean, Goni et al., (2011) found a poleward shift and amplified warming in the Brazil Current during 1993-2008 using satellite derived sea surface height anomaly and SST data. Similarly in the Indian Ocean, Biastoch et al., (2009) found warming near Southern Africa associated with an intensification of the Agulhas leakage. Later, Wu et al., (2012) presented a comprehensive analysis of the surface changes in these WBCs using satellite observations and found a strong warming over all these western boundary current regions over the last few decades and suggested that this amplified warming over the WBC extension regions is likely driven by the spin-up of portions of the subtropical gyre circulations in the Southern Hemisphere. More recently, Yang et al., (2016) extended on this to include an assessment of changes in the WBCs using satellite observations and data from multiple Coupled Model Intercomparison Project 5 (CMIP5) models. Yang et al., (2016) found a strong warming over the WBC extension regions associated with intensification of the poleward extensions of the WBCs in the Southern Hemisphere in both the satellite observations as well as historical simulations and future projections using the moderate emission scenario (Representative Concentration Pathway (RCP4.5)) from the CMIP5. They suggested that the changes in the WBC extension regions are primarily driven by changes in the near surface wind stress curl which are driven by a poleward shift in the surface westerly winds in the Southern Hemisphere extratropics associated with positive trend in the Southern Annular Mode (SAM).

The westerly wind jet in the Southern Hemisphere extratropics has intensified and moved poleward in the last few decades with strongest changes observed during austral summer. This is driven primarily by the springtime stratospheric ozone depletion with a secondary role played by the increasing greenhouse gases, both of which affect meridional temperature gradients in the atmosphere (Arblaster and Meehl, 2006; Swart et al., 2015). The Southern Hemisphere surface westerlies are projected to intensify and move further poleward in the future (Goyal et al., 2021a) which are projected to cause further intensification of the poleward portions of the Southern Hemisphere subtropical WBCs in the future (Sen Gupta et al., 2021; Oliver & Holbrook, 2014; Yang et al., 2016).

Several studies in the past have examined the role of projected future changes in the Southern Hemisphere extratropical surface westerly wind jet on the warming of the subtropical WBC extension regions in the Southern Hemisphere (Duran et al., 2020; Oliver & Holbrook, 2014; Yang et al., 2016). Variability and changes in the Southern Hemisphere westerly wind jet are often considered zonally symmetric because of the absence of major land and orographic features in the Southern Hemisphere extratropics, however, there are important zonal asymmetries present in the flow such as the Zonal Wave 3 (Goyal et al., 2021b; Raphael, 2004), Zonal Wave 1 (Raphael, 1998) and the Amundsen Sea Low (Goyal et al., 2021c). Because of this, many ocean model studies (e.g., Delworth & Zeng, 2008; Downes et al., 2017; Frankcombe et al., 2013; Hogg et al., 2017; Spence et al., 2014; Waugh et al., 2019; to name a few) examine future changes in the Southern Ocean by explicitly applying zonally symmetric future wind forcing over the Southern Hemisphere extratropics. While this assumption may be reasonable to first order, past and projected future changes in the Southern Hemisphere atmospheric circulation also contain significant regional variations

(zonal asymmetries) which may play an important role in driving different regional responses in the Southern Ocean (Goyal et al., 2021a). Although few recent studies (e.g., Waugh et al., 2020; Goyal et al., 2021a) have emphasized the presence of strong zonal asymmetries in both the past and projected changes in the Southern Hemisphere atmospheric circulation, the importance of these zonal asymmetries have yet to be quantified for the Southern Ocean. In this study, we use an ocean-sea-ice model forced with prescribed atmospheric fields to isolate the role played by the future zonally symmetric and asymmetric components of atmospheric changes in surface warming and ocean circulation changes focusing on the Southern Ocean subtropical WBC regions.

2. Methods

Ocean model

We use the Australian Community Climate Earth System Simulator - Ocean Model 2 v1.0 (ACCESS-OM2) coupled ocean-sea-ice model (Kiss et al., 2020). The model has a 360x300 horizonal mesh with a 1° zonal grid spacing. The meridional grid spacing is adjusted based on the cosine of the latitude and also incorporates a refinement to 1/3° within 10° of the Equator. More details on how the meridional grid spacing is computed can be obtained from Bi et al., (2013). ACCESS-OM2 consists of two-way coupled ocean and sea-ice models which are driven by the prescribed atmospheric forcing. The ocean model component is the Modular Ocean Model (MOM) version 5.1 from the Geophysical Fluid Dynamics Laboratory (Griffies, 2012) and the sea-ice model component is the Los Alamos sea-ice model (CICE) version 5.1.2 from Los Alamos National Laboratories (Hunke et al., 2015). The model components are coupled using the Ocean Atmosphere Sea Ice Soil (OASIS3-MCT) version 2.0 from CERFACS and CNRS, France (Valcke et al., 2015). In the horizontal direction, both MOM5 and CICE5 use the same

orthogonal curvilinear Arakawa B grid with velocity components co-located at the northeast corner of tracer cells. The model has 50 levels in the vertical with 2.3 m spacing at the surface, increasing smoothly to 219.6 m at the bottom at 5363.5 meters. Detailed information about ACCESS-OM2 can be obtained from Kiss et al., (2020).

In this study we are particularly interested in evaluating the ocean component of future projections in relation to the role of zonally-symmetric vs. zonally-asymmetric Southern Hemisphere atmospheric forcing trends. With CMIP5 and CMIP6 projections typically run using ~1° horizontal resolution ocean models, we also employ a 1-degree global ocean model to explore the ocean response to zonally symmetric and asymmetric forcing at the latitude of the Southern Hemisphere westerly wind belt. While coarse resolution models clearly lack important physics, particularly in high energy areas like WBCs, previous higher-resolution ocean and regional coupled model experiments, forced with projected changes from CMIP models, show qualitatively similar ocean circulation responses to the CMIP models (e.g., Biastoch & Böning, 2013; Bull et al., 2020; Feng et al., 2017; Oliver & Holbrook, 2014).

Model simulations

ACCESS-OM2 is forced with atmospheric forcing fields obtained from the ACCESS Coupled Model version 2 (ACCESS-CM2) coupled climate model (Bi et al., 2020) which is a part of the Coupled Model Intercomparison Project 6 (CMIP6) of the Intergovernmental Panel on Climate Change (IPCC). A model spin-up is first carried out for 520 years by forcing the model with a repeat cycle of the daily atmospheric forcing fields using a reference 40-year period of data obtained from the pre-industrial control simulation of the ACCESS-CM2. Three 80-yr simulations are branched from year 520 of the spin up. The first simulation (*CTRL*)

compromises two additional 40-yr cycles of the same daily surface forcing as the spin-up. The second simulation (*Future* simulation) is similar except an offset is added to the surface forcing. This offset represents the change in the mean state and seasonal cycle between the pre-industrial period and 2081-2100 under the high emission scenario of the CMIP6 (Shared Socio-economic pathway (SSP5-8.5)). This change in the surface forcing is calculated as the difference between the 2081-2100 monthly mean climatology and the associated climatology from the 40-yr pre-industrial reference period (refer to Fig. 1 and Fig. S1 for the surface forcing offset used in the *Future* simulation). The full surface forcing for the *Future* simulation is then comprised of the same 40 years of daily forcing used by the *CTRL* experiment, but with the repeat climatological monthly mean future projections superimposed. The 2081-2100 climatology is calculated using the average of 3 ensemble members of ACCESS-CM2 subject to SSP5-8.5 forcing, to reduce contamination by low frequency variability. By using this atmospheric forcing, the daily variability is the same between all experiments, and any changes can be related to changes in the mean state or the seasonal cycle. The third simulation (*Symmetric*) is similar to the *Future* simulation, but it incorporates the *zonal mean* of the *Future* surface forcing poleward of 25°S (refer to Fig. 1 and Fig. S2 for the surface forcing offset used in the simulation and Fig. S3 for the projected zonally asymmetric atmospheric changes). To eliminate any sudden gradients in the data by imposing a zonal mean anomaly south of 25°S, a buffer region has been used and a linear tapering is applied between 20-25°S. Only the last 40 years of each of the three experiments are used to allow time for the ocean to adjust to the change in forcing.

All results presented show the differences between the two future simulations and the *CTRL* simulation to account for any spurious drift in the model simulations. Therefore, differences

between the *Future* and *CTRL* simulations provide an estimate of the "total" projected changes and differences between the *Symmetric* and *CTRL* simulations provide an estimate of the changes only related to the zonally symmetric atmospheric changes in the Southern Hemisphere extratropics. Future changes related to the zonally asymmetric atmospheric changes only are estimated as a difference between the *Future* and *Symmetric* simulations.

3. Surface warming of the subtropical western boundary current regions

Consistent with previous studies (e.g., Xie, 2020; Yang et al., 2016), we find warming throughout the Southern Ocean and a substantially amplified warming in the poleward extensions of the subtropical western boundary current regions in the *Future* simulation (Fig. 2a). In particular, strong warming is found in the Brazil and Malvinas confluence and the EAC extension regions while a more muted warming occurs in the Agulhas Current region. When only zonally symmetric future atmospheric anomalies are prescribed south of 25°S, a similar SST warming signature is found (Fig. 2b) suggesting that to first order, the future changes in the Southern Ocean SST warming are driven by the zonally symmetric changes in the atmospheric forcing. However, zonal asymmetries play an important role in certain regions of the Southern Ocean (Fig. 2c). It is interesting to note that out of all the three major warming regions (subtropical WBC extension regions), the Brazil and Malvinas confluence region is the only one where the SST warming is almost completely explained by zonally symmetric atmospheric changes. In contrast, the *Symmetric* simulation shows strong reduction in warming as compared to the *Future* simulation in the region South of Australia and in the Tasman Sea and also shows somewhat muted warming in the Agulhas Current region (Fig. 2b). These regional differences may arise from the fact that the zonal asymmetries in the atmospheric fields, in particular the winds, are strongest in the Pacific, followed by the Indian

Ocean and are relatively weak in the Atlantic Ocean (Fig. 1). The zonally asymmetric atmospheric changes accounts for more than 30% of the ocean warming in parts of the Tasman Sea and a weaker warming over the Agulhas Current region (Fig. 2c). We anticipate that changes in the ocean circulation may play an important role in driving these changes. This will be investigated in the next section.

An extensive area of relatively weak warming extends across the southeast Pacific in the *Future* simulation between 20-40°S (Fig. 2a). This patch vanishes in the *Symmetric* simulation (Fig. 2b) and is therefore visible as a strong cooling SST anomaly associated with zonally asymmetric forcing (Fig. 2c). A collocated area of weak prescribed surface air temperature warming is also found in the *Future* simulation (Fig. 1g) which vanishes in the *Symmetric* case as the zonal mean anomaly is applied (Fig. 1h). The cooling SST anomaly in the zonally asymmetric case is related to the collocated prescribed surface air temperature forcing. Moreover, no substantial changes in the oceanic heat transport were found in this region (not shown). As the zonally asymmetric component of the atmospheric forcing only has strong effects in the Indian and the Pacific Ocean with little influence in the Atlantic Ocean (Fig. 2c), we now focus only on the projected changes in the Indo-Pacific region.

4. Projected changes in ocean circulation

To help understand the changes in the projected SST warming in the WBC extension regions, we next examine changes in the upper ocean western boundary currents (vertically integrated from 0-100 meters as a proxy for the mixed layer depth) to determine if changes in the strength of the subtropical western boundary currents in the Indian and the Pacific Ocean are important for the amplification of the ocean SST warming. In the Pacific, an intense

EAC is found in the *CTRL* simulation which flows from tropical latitudes southward until most of the current retroflects eastward as the Tasman front at approximately 32°S (Fig. 3a). Direction of flow of these currents does not change when integrated to a deeper depth (refer to Fig. S4 for 0-1000 m depth integrated currents). In the *Future* simulation, while the EAC north of 30°S and the Tasman front are projected to weaken slightly, a substantial strengthening of the EAC extension and Tasman leakage flowing westward south of Tasmania, is projected. These results are consistent with previous studies which found similar projected changes in the subtropical western boundary currents in the Pacific Ocean using multiple CMIP5 and CMIP6 models (Sen Gupta et al., 2021). When only zonally symmetric future atmospheric changes are prescribed, similar but weaker changes are found along the EAC, Tasman front, EAC extension and the Tasman Leakage (Fig. 3e). Although zonally symmetric anomalies appear to drive the majority of changes in the Pacific basin, more than 30% of the ocean current changes along the major flow pathways are associated with the zonally asymmetric atmospheric changes (Fig. 3g).

In the Indian Ocean, a strong Agulhas Current in the upper ocean (0-100m) is found in the *CTRL* simulation flowing poleward from the tropical latitudes between Madagascar and the mainland (Fig. 3b). After breaking away from the coast near the southern tip of Africa, the Agulhas Current retroflects eastward and flows as the Agulhas return Current. A part of the Agulhas Current also flows westward from the retroflection point as the Agulhas leakage (Fig. 3b, refer to Fig. S4 for 0-1000m depth integrated current). Another albeit weaker WBC, the East Madagascar Current (EMC), is found in the Indian Ocean flowing poleward to the east of Madagascar, before retroflecting eastward after reaching the southern tip of Madagascar (Fig. 3b, Fig. S4). A small portion of the EMC also connects with the Agulhas Current in the

region south of Madagascar and flows eastward from the Agulhas Current to the EMC extension (Fig. 3b). When integrated from surface to 1000 meters depth, the EMC turns westward after reaching south of Madagascar and feeds into the Agulhas Current (Fig. S4) consistent with observations (Davis, 2005).

In the *Future* simulation, a weakening of the Agulhas Current close to the southern tip of Africa is found with little change found in the Agulhas Current further north (Fig. 3d). An increase in the Agulhas leakage and weakening of the eastward retroflected Agulhas return current along with a weakening of both the EMC as well as its extension are also found in the *Future* simulation (Fig. 3d). While most of the changes in the Agulhas leakage, Agulhas return Current, the EMC and its extension are reproduced in the *Symmetric* simulation, the asymmetric forcing components appear to counteract some of the changes simulated to the west and south of Mozambique in the *Symmetric* simulation, also causing a small additional weakening of the retroflection (Fig. 3f, 3h). Flow in the region connecting the Agulhas Current and the EMC is also projected to strengthen in the *Future* simulation and this change seems to be largely driven by zonally asymmetric atmospheric changes (Fig. 3h).

5. Changes in volume and heat transport

Strengthening of the EAC extension and weakening of the Tasman front in the *Future* simulation results in an increase in the poleward volume and heat transport of warm subtropical waters into the Tasman Sea (Fig. 4a, c). Most of this additional subtropical water and about half of the additional heat leaves the Tasman Sea via an intensified Tasman leakage in the *Future* simulation (Fig. 4a) resulting in more heat being transported westwards in the region south of Australia (Fig. 4c) with a small amount of additional transport of heat

296 polewards. Overall, there is net heat gain in the Tasman Sea region (Fig. 4a, 4c). This heat gain
297 from ocean advection is then lost to the atmosphere by surface heat fluxes (Fig. 4c). The small
298 residuals found after adding the advection and surface heat flux terms would be due to
299 vertical processes (i.e., diffusion and upwelling) at the bottom of the box (at 100-meters
300 depth) and errors associated with using monthly-averaged temperature and velocity fields.
301 Similar sign changes in the volume and heat transport compared to the *Future* simulation can
302 be seen for both the zonally symmetric and asymmetric forcing anomalies, with asymmetric
303 atmospheric changes alone contributing close to 30% of the total changes in the poleward
304 heat and volume transport on the equatorward side of the box (Fig. 4a, 4c).
305
306 In the Indian Ocean, the Agulhas circulation weakens slightly in the *Future* simulation with
307 more weakening poleward of 33°S as compared to the northern part of the current. This
308 results in less warm water entering from the north via the Agulhas Current and less water
309 feeding southward on the poleward side of the box which is compensated by more water
310 escaping towards the east in the *Future* simulation as compared to the *CTRL* simulation (Fig.
311 4b, 4d). The net result from the ocean advection is a net heat gain in this region (shown by a
312 box in Fig. 4d) which is balanced by additional heat loss to the atmosphere in the *Future*
313 simulation (Fig. 4d). Here again, small residuals are found which are due to changes in the
314 vertical fluxes across 100-meters depth. Similar to the *Future* simulation, the Agulhas Current
315 is found to weaken in the future in the *Symmetric* simulation. However, more weakening on
316 the northward edge of the box and a muted weakening on the poleward side of the box is
317 found in the *Symmetric* simulation as compared to the *Future* simulation (Fig. 4b). This results
318 in net poleward heat transport on the northward edge of the box due to projected zonally
319 asymmetric atmospheric forcing (Fig. 4d). On the eastern and southern edges, changes in the

heat and volume transport are primarily related to the asymmetric component of forcing (Fig. 4b, 4d). The result is a net heat gain from advection of heat due to zonally asymmetric forcing which is balanced by additional heat loss to the atmosphere (Fig. 4d).

6. Changes in the large-scale ocean circulation

Next we look more broadly at the basin scale changes in the Southern Hemisphere subtropical gyre circulations. To do this, we investigate changes in the barotropic streamfunction (Fig. 5a-f). In the Pacific basin, there is a cyclonic anomaly to the north and an anticyclonic anomaly to the south in the *Future* simulation as compared to the *CTRL* simulation which means that the EAC core and the Tasman front are projected to weaken and the EAC extension and the Tasman leakage are projected to strengthen in the *Future* simulation (Fig. 5a) which agrees well with the transports derived from the upper 100 meters (Fig. 4a, 4c). This highlights that the common description of a future intensification of the South Pacific subtropical gyre is misleading as the strengthening is only projected in the southern part of the gyre (Fig. 5a). Here again, the *Symmetric* simulation reproduces a large part of this change in the barotropic streamfunction (Fig. 5c). However, future zonally asymmetric atmospheric changes also account for a substantial part of the total future changes in the barotropic streamfunction with a reduced gyral circulation north of ~28°S and an amplified circulation south of this latitude (Fig. 4a, 5e).

In the Indian Ocean, there is also a cyclonic anomaly to the north and an anticyclonic anomaly to the south in the *Future* simulation (Fig. 5b). Most of the changes in the barotropic streamfunction found in the *Future* simulation can be explained by the zonally symmetric changes (Fig. 5d). However, asymmetric atmospheric changes result in a weak cyclonic

anomaly off southeast Africa that acts to reduce southward volume transport and a weak anticyclonic anomaly near Madagascar that acts to increase southward volume transport (Fig. 5f). This translates to increased poleward transport of warm tropical water from the north and reduced poleward volume transport to the south, resulting in warm SST anomalies in the region (Fig. 4d).

To examine the cause of the ocean circulation changes, we calculate the Sverdrup streamfunction by zonally integrating the surface wind stress curl in each ocean. More sophisticated approaches are possible where effects due to the presence of islands (e.g., New Zealand and Madagascar) are considered while computing the Sverdrup streamfunction (e.g., Island rule calculations using Godfrey, 1989). However, these island rule calculations are known to not perform well in the South Pacific (Wajsowicz, 1993). To first order the barotropic circulation can be understood in terms of changes in the surface winds via Sverdrup theory. Both the mean Sverdrup circulation and the asymmetric component of the change (Fig. 5g, h) are qualitatively similar to the corresponding barotropic streamfunction (Fig. 5e, f). In particular, off Australia, we find a reduction in the southward volume transport at ~25°S and an increase in the southward volume transport at ~32°S (Fig. 5g). Similarly, in the Indian Ocean, we find an increase in the southward volume transport at ~25°S and a reduction in the southward volume transport at ~32°S, consistent with the changes in the barotropic streamfunction because of the projected zonally asymmetric atmospheric changes in this region (Fig. 5h).

7. Summary and Discussions

An ocean-sea-ice model forced by prescribed atmospheric fields is used to examine the relative importance of zonally symmetric vs. zonally asymmetric atmospheric changes for future projected upper ocean changes in the Southern Hemisphere mid-latitudes. We found that the projected changes are largely driven by the zonally symmetric component of the forcing, however, zonally asymmetric atmospheric changes play a substantial role in generating projected changes in the Indian as well as Pacific Ocean basins. The zonally asymmetric component of forcing can itself explain more than 30% (>2°C) of the projected SST warming in the Tasman Sea and south Australia region and a sizeable fraction of warming in the Agulhas Current region. These changes are likely driven by the changes in the ocean circulation in both these ocean basins due to zonally asymmetric atmospheric changes, which results in an increase in the poleward transport of warm subtropical water to the Southern Hemisphere mid-latitudes. An increase in the poleward transport of warm subtropical water leads to net heat gain in the Tasman Sea and southeast Africa regions. Investigation of changes in the Sverdrup circulation resulting from changes to the surface wind stress curl suggests that the total projected changes in the ocean circulation are related to both the zonally symmetric as well as zonally asymmetric changes in the atmospheric circulation. Sverdrup calculation also shows that the zonal asymmetries in the wind forcing as opposed to zonal asymmetries in the surface heat fluxes can explain the changes in the ocean circulation.

A potential issue with our experimental design is the possibility of spurious wind stress curl anomalies at the boundary between 20-25°S in the *Symmetric* simulation. To test this, we conduct another simulation in which we apply zonal mean future anomalies at all latitudes.

We found very little difference in the magnitude of projected SST warming indicating that zonally asymmetric circulation changes further north have little impact on the results presented in this study (Fig. S5).

We calculate the contribution of projected zonally asymmetric atmospheric changes by subtracting the changes in the *Symmetric* simulation from the *Future* simulation and therefore assume that the symmetric and asymmetric components combine linearly to give the total response. However, their responses may not be independent of each other. For instance, the unprecedented 2015-16 Antarctic sea-ice decline event was linked to the presence of a strong zonal wavenumber 3 in the Southern Hemisphere extratropical atmospheric circulation (Meehl et al., 2019; Purich & England, 2019; Wang et al., 2019), however, its influence on the Antarctic sea-ice may have been affected by the poleward contracting zonal mean westerly wind jet in the Southern Hemisphere. This issue of non-linearity has not been discussed here and can be possibly addressed in future studies.

As the future atmospheric circulation changes over the Southern Hemisphere extratropics are largely zonally symmetric, ocean modelling studies carried out to examine projected ocean changes (associated with variability and long term changes) have often prescribed zonally symmetric projected atmospheric forcing (e.g., Delworth & Zeng, 2008; Downes et al., 2017; Frankcombe et al., 2013; Hogg et al., 2017; Spence et al., 2014; Waugh et al., 2019 to name a few). Goyal et al., (2021a) showed substantial zonal asymmetries in the projected surface westerly winds in the Southern Hemisphere extratropics using multiple CMIP5 and CMIP6 models. Here we show that these zonal asymmetries are important and can explain a substantial fraction of the upper ocean changes in the Pacific and Indian Ocean basins. Our

results thus suggest that prescribing a zonal mean wind anomaly may underestimate future upper ocean changes particularly in the subtropical WBC extension regions. Instead, full zonally-varying atmospheric anomalies should be used to examine the role of future atmospheric changes over the region. While we acknowledge that different models can show large diversity in their projected responses (Sen Gupta et al., 2021), this study demonstrates that zonal asymmetries in future changes can in principle have large impacts on regional circulation change.

Acknowledgements

This study was supported by the Australian Research Council (grants CE170100023, FL150100035). R.G. is supported by the Scientia PhD scholarship from the University of New South Wales. M.H.E. is also supported by the Earth Science and Climate Change Hub of the Australian Government's National Environmental Science Programme (NESP) and the Centre for Southern Hemisphere Oceans Research (CSHOR), a joint research centre between QNLM, CSIRO, UNSW and UTAS. All the model simulations and analysis were conducted on the National Computational Infrastructure (NCI) facility based in Canberra, Australia.

Data availability statement

ACCESS-CM2 data used to force the ocean model simulations can be downloaded from the Earth System Grid Federation (ESGF) - https://esgf-node.llnl.gov/search/cmip6/. Data from the ocean model simulations required to reproduce the results presented in this study has been made available and can be freely download from https://data.mendeley.com/datasets/7sw7kf8nxk/draft?a=b9062eee-4582-4187-948d-cbd194901206.

References

Bi, D., Marsland, S., Uotila, P., O'Farrell, S., Fiedler, R., Sullivan, A., et al. (2013). ACCESS-OM: the ocean and sea-ice core of the ACCESS coupled model. *Australian Meteorological and Oceanographic Journal*, *63*(1), 213–232. https://doi.org/10.22499/2.6301.014

Bi, D., Dix, M., Marsland, S., O'Farrell, S., Sullivan, A., Bodman, R., et al. (2020). Configuration and spin-up of ACCESS-CM2, the new generation Australian Community Climate and Earth System Simulator Coupled Model. *Journal of Southern Hemisphere Earth Systems Science*, *70*(1), 225. https://doi.org/10.1071/ES19040

Biastoch, A, Böning, C. W., Schwarzkopf, F. U., & Lutjeharms, J. R. E. (2009). Increase in Agulhas leakage due to poleward shift of Southern Hemisphere westerlies. *Nature*, *462*(7272), 495–498. https://doi.org/10.1038/nature08519

Biastoch, A., & Böning, C. W. (2013). Anthropogenic impact on Agulhas leakage. *Geophysical Research Letters*, *40*(6), 1138–1143. https://doi.org/10.1002/grl.50243

Bull, C. Y. S., Kiss, A. E., Gupta, A. Sen, Jourdain, N. C., Argüeso, D., Di Luca, A., & Sérazin, G. (2020). Regional Versus Remote Atmosphere-Ocean Drivers of the Rapid Projected Intensification of the East Australian Current. *Journal of Geophysical Research: Oceans*, *125*(7), e2019JC015889. https://doi.org/10.1029/2019JC015889

Cronin, M. F., Cronin, M. F., Cronin, M. F., Cronin, M. F., Cronin, M. F., Cronin, M. F., et al. (2010). Monitoring Ocean - Atmosphere Interactions in Western Boundary Current Extensions. In *Proceedings of OceanObs'09: Sustained Ocean Observations and Information for Society* (pp. 199–209). European Space Agency. https://doi.org/10.5270/OceanObs09.cwp.20

Davis, R. E. (2005). Intermediate-Depth Circulation of the Indian and South Pacific Oceans Measured by Autonomous Floats. *Journal of Physical Oceanography*, *35*(5), 683–707. https://doi.org/10.1175/JPO2702.1

Delworth, T. L., & Zeng, F. (2008). Simulated impact of altered Southern Hemisphere winds on the Atlantic Meridional Overturning Circulation. *Geophysical Research Letters*, *35*(20), L20708. https://doi.org/10.1029/2008GL035166

Downes, S. M., Langlais, C., Brook, J. P., & Spence, P. (2017). Regional Impacts of the Westerly Winds on Southern Ocean Mode and Intermediate Water Subduction. *Journal of Physical Oceanography*, *47*(10), 2521–2530. https://doi.org/10.1175/JPO-D-17-0106.1

Dubois, M., Rossi, V., Ser-Giacomi, E., Arnaud-Haond, S., López, C., & Hernández-García, E. (2016). Linking basin-scale connectivity, oceanography and population dynamics for the conservation and management of marine ecosystems. *Global Ecology and Biogeography*, *25*(5), 503–515. https://doi.org/10.1111/geb.12431

Duran, E. R., England, M. H., & Spence, P. (2020). Surface Ocean Warming Around Australia Driven by Interannual Variability and Long-Term Trends in Southern Hemisphere Westerlies. *Geophysical Research Letters*, *47*(9), e2019GL086605. https://doi.org/10.1029/2019GL086605

Eriksen, M., Maximenko, N., Thiel, M., Cummins, A., Lattin, G., Wilson, S., et al. (2013). Plastic pollution in the South Pacific subtropical gyre. *Marine Pollution Bulletin*, *68*(1–2), 71–76. https://doi.org/10.1016/j.marpolbul.2012.12.021

Everett, J. D., Sebille, E., Taylor, M. D., Suthers, I. M., Setio, C., Cetina-Heredia, P., & Smith, J. A. (2017). Dispersal of Eastern King Prawn larvae in a western boundary current: New insights from particle tracking. *Fisheries Oceanography*, *26*(5), 513–525.

https://doi.org/10.1111/fog.12213
Feng, M., Zhang, X., Sloyan, B., & Chamberlain, M. (2017). Contribution of the deep ocean to the centennial changes of the Indonesian Throughflow. *Geophysical Research Letters*, *44*(6), 2859–2867. https://doi.org/10.1002/2017GL072577
Frankcombe, L. M., Spence, P., Hogg, A. M., England, M. H., & Griffies, S. M. (2013). Sea level changes forced by Southern Ocean winds. *Geophysical Research Letters*, *40*(21), 5710–5715. https://doi.org/10.1002/2013GL058104
Ganachaud, A., & Wunsch, C. (2003). Large-Scale Ocean Heat and Freshwater Transports during the World Ocean Circulation Experiment. *Journal of Climate*, *16*(4), 696–705. https://doi.org/10.1175/1520-0442(2003)016<0696:LSOHAF>2.0.CO;2
Godfrey, J. S. (1989). A sverdrup model of the depth-integrated flow for the world ocean allowing for island circulations. *Geophysical & Astrophysical Fluid Dynamics*, *45*(1–2), 89–112. https://doi.org/10.1080/03091928908208894
Goni, G. J., Bringas, F., & DiNezio, P. N. (2011). Observed low frequency variability of the Brazil Current front. *Journal of Geophysical Research*, *116*(C10), C10037. https://doi.org/10.1029/2011JC007198
Goyal, R., Sen Gupta, A., Jucker, M., & England, M. H. (2021a). Historical and Projected Changes in the Southern Hemisphere Surface Westerlies. *Geophysical Research Letters*, *48*(4), e2020GL090849. https://doi.org/https://doi.org/10.1029/2020GL090849
Goyal, R., Jucker, M., Gupta, A. Sen, Hendon, H., & England, M. (2021b). Zonal Wave 3 Pattern in the Southern Hemisphere generated by tropical convection. *Nature Geoscience (in Press)*. https://doi.org/10.21203/rs.3.rs-320008/v1
Goyal, R., Jucker, M., Sen Gupta, A., & England, M. H. (2021c). Generation of the Amundsen Sea Low by Antarctic Orography. *Geophysical Research Letters*, *48*(4), e2020GL091487. https://doi.org/10.1029/2020GL091487
Griffies, S. M. (2012). Elements of the Modular Ocean Model (MOM). *GFDL Model Documentation*, *3*(C), 1–631.
Sen Gupta, A., Stellema, A., Pontes, G. M., Taschetto, A. S., Vergés, A., & Rossi, V. (2021). Future changes to the upper ocean Western Boundary Currents across two generations of climate models. *Scientific Reports*, *11*(1), 9538. https://doi.org/10.1038/s41598-021-88934-w
Hogg, A. M., Spence, P., Saenko, O. A., & Downes, S. M. (2017). The Energetics of Southern Ocean Upwelling. *Journal of Physical Oceanography*, *47*(1), 135–153. https://doi.org/10.1175/JPO-D-16-0176.1
Hunke, E. C., Lipscomb, W. H., Turner, A. K., Jeffery, N., & Elliot, S. (2015). CICE : the Los Alamos Sea Ice Model Documentation and Software User's Manual Version 5.1 LA-CC-06-012. *Los Alamos National Laboratory Tech. Rep. LA-CC-06-012*, (March 17), 76.
Kiss, A. E., Hogg, A. M., Hannah, N., Boeira Dias, F., Brassington, G. B., Chamberlain, M. A., et al. (2020). ACCESS-OM2 v1.0: a global ocean–sea ice model at three resolutions. *Geoscientific Model Development*, *13*(2), 401–442. https://doi.org/10.5194/gmd-13-401-2020
Kwon, Y.-O., Alexander, M. A., Bond, N. A., Frankignoul, C., Nakamura, H., Qiu, B., & Thompson, L. A. (2010). Role of the Gulf Stream and Kuroshio–Oyashio Systems in Large-Scale Atmosphere–Ocean Interaction: A Review. *Journal of Climate*, *23*(12), 3249–3281. https://doi.org/10.1175/2010JCLI3343.1
Meehl, G. A., Arblaster, J. M., Chung, C. T. Y., Holland, M. M., DuVivier, A., Thompson, L., et al. (2019). Sustained ocean changes contributed to sudden Antarctic sea ice retreat in

late 2016. *Nature Communications*, *10*(1), 14. https://doi.org/10.1038/s41467-018-07865-9

Minobe, S., Kuwano-Yoshida, A., Komori, N., Xie, S.-P., & Small, R. J. (2008). Influence of the Gulf Stream on the troposphere. *Nature*, *452*(7184), 206–209. https://doi.org/10.1038/nature06690

Oliver, E. C. J., & Holbrook, N. J. (2014). Extending our understanding of South Pacific gyre "spin-up": Modeling the East Australian Current in a future climate. *Journal of Geophysical Research: Oceans*, *119*(5), 2788–2805. https://doi.org/10.1002/2013JC009591

Purich, A., & England, M. H. (2019). Tropical Teleconnections to Antarctic Sea Ice During Austral Spring 2016 in Coupled Pacemaker Experiments. *Geophysical Research Letters*, *46*(12), 6848–6858. https://doi.org/10.1029/2019GL082671

Raphael, M. N. (2004). A zonal wave 3 index for the Southern Hemisphere. *Geophysical Research Letters*, *31*(23). https://doi.org/10.1029/2004GL020365

Raphael, Marilyn N. (1998). Quasi-Stationary Waves in the Southern Hemisphere: An Examination of Their Simulation by the NCAR Climate System Model, with and without an Interactive Ocean*. *Journal of Climate*, *11*(6), 1405–1418. https://doi.org/10.1175/1520-0442(1998)011<1405:QSWITS>2.0.CO;2

Ridgway, K. R. (2007). Long-term trend and decadal variability of the southward penetration of the East Australian Current. *Geophysical Research Letters*, *34*(13), n/a-n/a. https://doi.org/10.1029/2007GL030393

Ridgway, K. R., Coleman, R. C., Bailey, R. J., & Sutton, P. (2008). Decadal variability of East Australian Current transport inferred from repeated high-density XBT transects, a CTD survey and satellite altimetry. *Journal of Geophysical Research*, *113*(C8), C08039. https://doi.org/10.1029/2007JC004664

Roemmich, D., Gilson, J., Davis, R., Sutton, P., Wijffels, S., & Riser, S. (2007). Decadal Spinup of the South Pacific Subtropical Gyre. *Journal of Physical Oceanography*, *37*(2), 162–173. https://doi.org/10.1175/JPO3004.1

Rossi, V., Van Sebille, E., Sen Gupta, A., Garçon, V., & England, M. H. (2013). Multi-decadal projections of surface and interior pathways of the Fukushima Cesium-137 radioactive plume. *Deep Sea Research Part I: Oceanographic Research Papers*, *80*, 37–46. https://doi.org/https://doi.org/10.1016/j.dsr.2013.05.015

Spence, P., Griffies, S. M., England, M. H., Hogg, A. M., Saenko, O. A., & Jourdain, N. C. (2014). Rapid subsurface warming and circulation changes of Antarctic coastal waters by poleward shifting winds. *Geophysical Research Letters*, *41*(13), 4601–4610. https://doi.org/10.1002/2014GL060613

Swart, N. C., Fyfe, J. C., Gillett, N., & Marshall, G. J. (2015). Comparing Trends in the Southern Annular Mode and Surface Westerly Jet. *Journal of Climate*, *28*(22), 8840–8859. https://doi.org/10.1175/JCLI-D-15-0334.1

Takahashi, T., Sutherland, S. C., Wanninkhof, R., Sweeney, C., Feely, R. A., Chipman, D. W., et al. (2009). Climatological mean and decadal change in surface ocean pCO2, and net sea–air CO2 flux over the global oceans. *Deep Sea Research Part II: Topical Studies in Oceanography*, *56*(8–10), 554–577. https://doi.org/10.1016/j.dsr2.2008.12.009

Valcke, S., Craig, T., & Coquart, L. (2015). OASIS3-MCT User Guide. *CERFACS/CNRS SUC URA No1875*, (May).

Wajsowicz, R. C. (1993). The Circulation of the Depth-integrated Flow around an Island with Application to the Indonesian Throughflow. *Journal of Physical Oceanography*, *23*(7),

1470–1484. https://doi.org/10.1175/1520-0485(1993)023<1470:TCOTDI>2.0.CO;2
Wang, G., Hendon, H. H., Arblaster, J. M., Lim, E.-P., Abhik, S., & van Rensch, P. (2019). Compounding tropical and stratospheric forcing of the record low Antarctic sea-ice in 2016. *Nature Communications*, *10*(1), 13. https://doi.org/10.1038/s41467-018-07689-7
Waugh, D. W., McC. Hogg, A., Spence, P., England, M. H., & Haine, T. W. N. (2019). Response of Southern Ocean Ventilation to Changes in Midlatitude Westerly Winds. *Journal of Climate*, *32*(17), 5345–5361. https://doi.org/10.1175/JCLI-D-19-0039.1
Waugh, D. W., Banerjee, A., Fyfe, J. C., & Polvani, L. M. (2020). Contrasting recent trends in Southern Hemisphere Westerlies across different ocean basins. *Earth and Space Science Open Archive*. https://doi.org/10.1002/essoar.10503156.1
Williams, R. G., & Follows, M. J. (2003). Physical Transport of Nutrients and the Maintenance of Biological Production BT - Ocean Biogeochemistry: The Role of the Ocean Carbon Cycle in Global Change. In M. J. R. Fasham (Ed.) (pp. 19–51). Berlin, Heidelberg: Springer Berlin Heidelberg. https://doi.org/10.1007/978-3-642-55844-3_3
Wu, L., Cai, W., Zhang, L., Nakamura, H., Timmermann, A., Joyce, T., et al. (2012). Enhanced warming over the global subtropical western boundary currents. *Nature Climate Change*, *2*(3), 161–166. https://doi.org/10.1038/nclimate1353
Xie, S. (2020). Ocean Warming Pattern Effect On Global And Regional Climate Change. *AGU Advances*, *1*(1). https://doi.org/10.1029/2019AV000130
Yang, H., Lohmann, G., Wei, W., Dima, M., Ionita, M., & Liu, J. (2016). Intensification and poleward shift of subtropical western boundary currents in a warming climate. *Journal of Geophysical Research: Oceans*, *121*(7), 4928–4945. https://doi.org/10.1002/2015JC011513

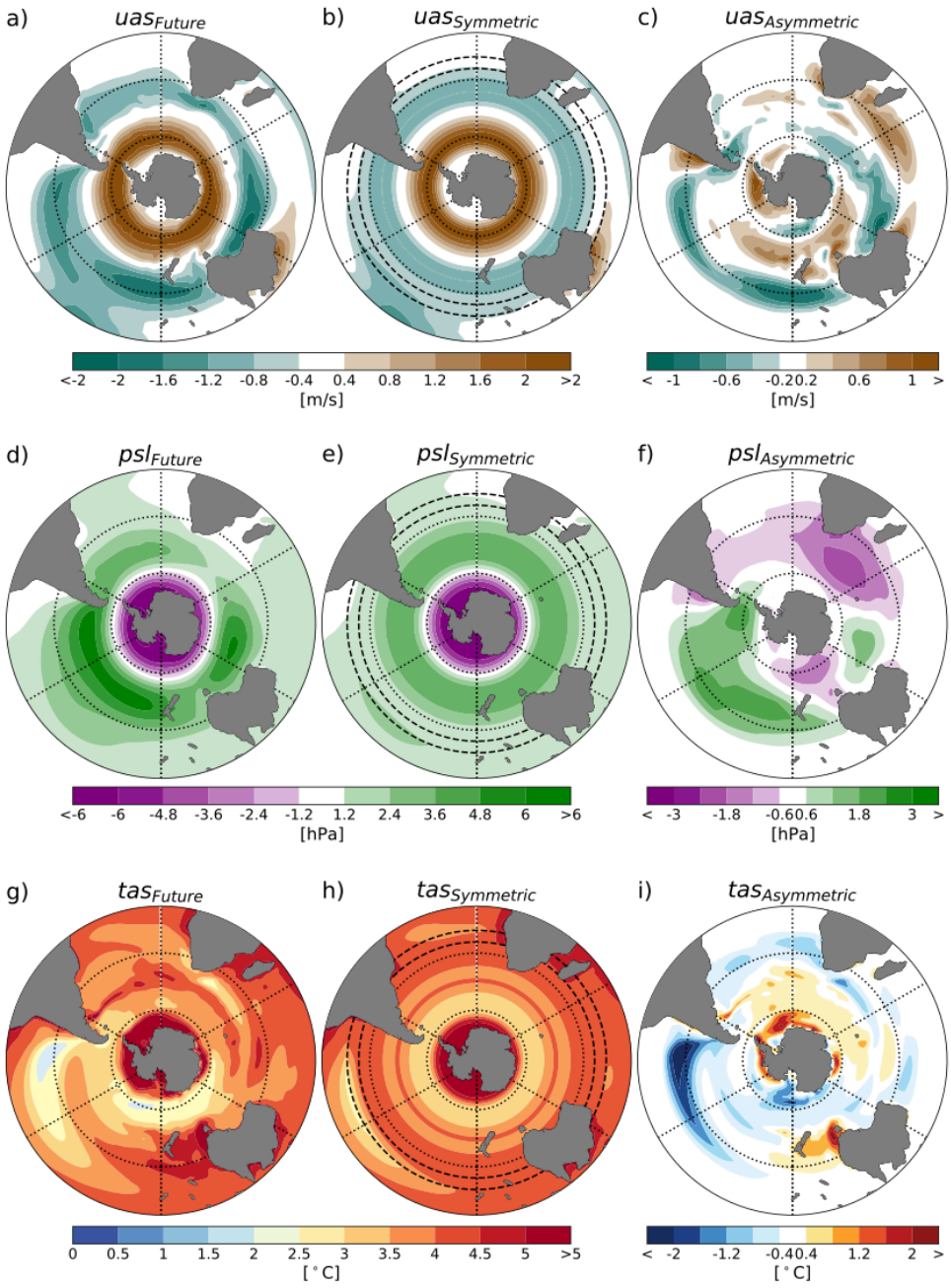

Figure 1 | End of the 21st Century (2081-2100 average) atmospheric field anomalies computed from the ACCESS-CM2 simulations. Left column shows full 2081-2100 annual averaged anomaly as the mean of three ensemble members used for *Future* simulation. Middle column shows the 2081-2100 annual averaged future anomaly for the Symmetric simulation where zonally symmetric anomaly is prescribed south of 25°S. Right column shows the difference between the left and the middle column. Top row represents zonal wind anomaly (uas), middle row represents mean sea level pressure anomaly (psl) and bottom row represents surface air temperature anomaly (tas). Thick dashed lines in the middle column represent the tapering region between the zonal mean anomalies south of 25°S and the full anomalies north of 20°S.

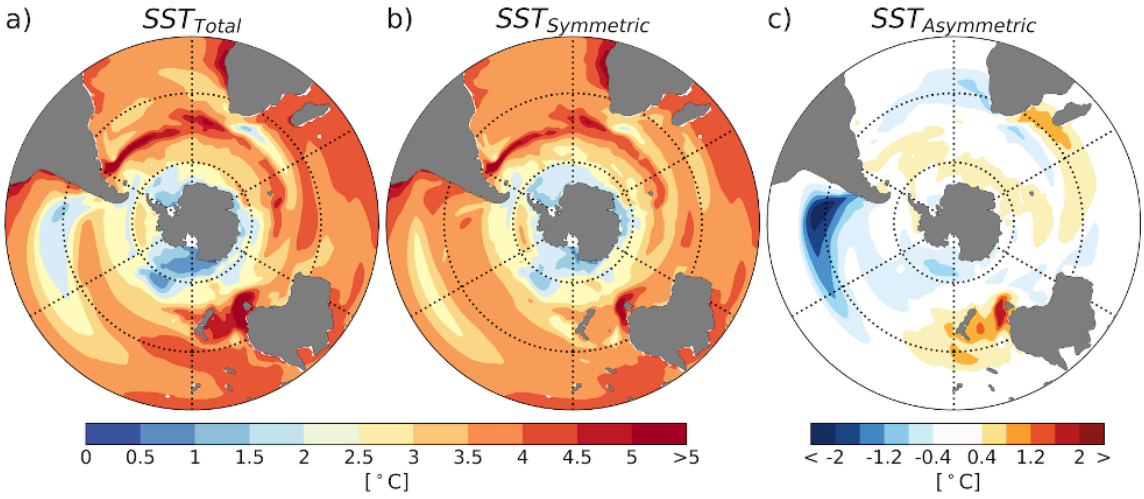

Figure 2 | Sea Surface Temperature (SST) change because of Total (panel a), Symmetric (panel b) and Asymmetric (panel c) atmospheric changes in the Southern Hemisphere.

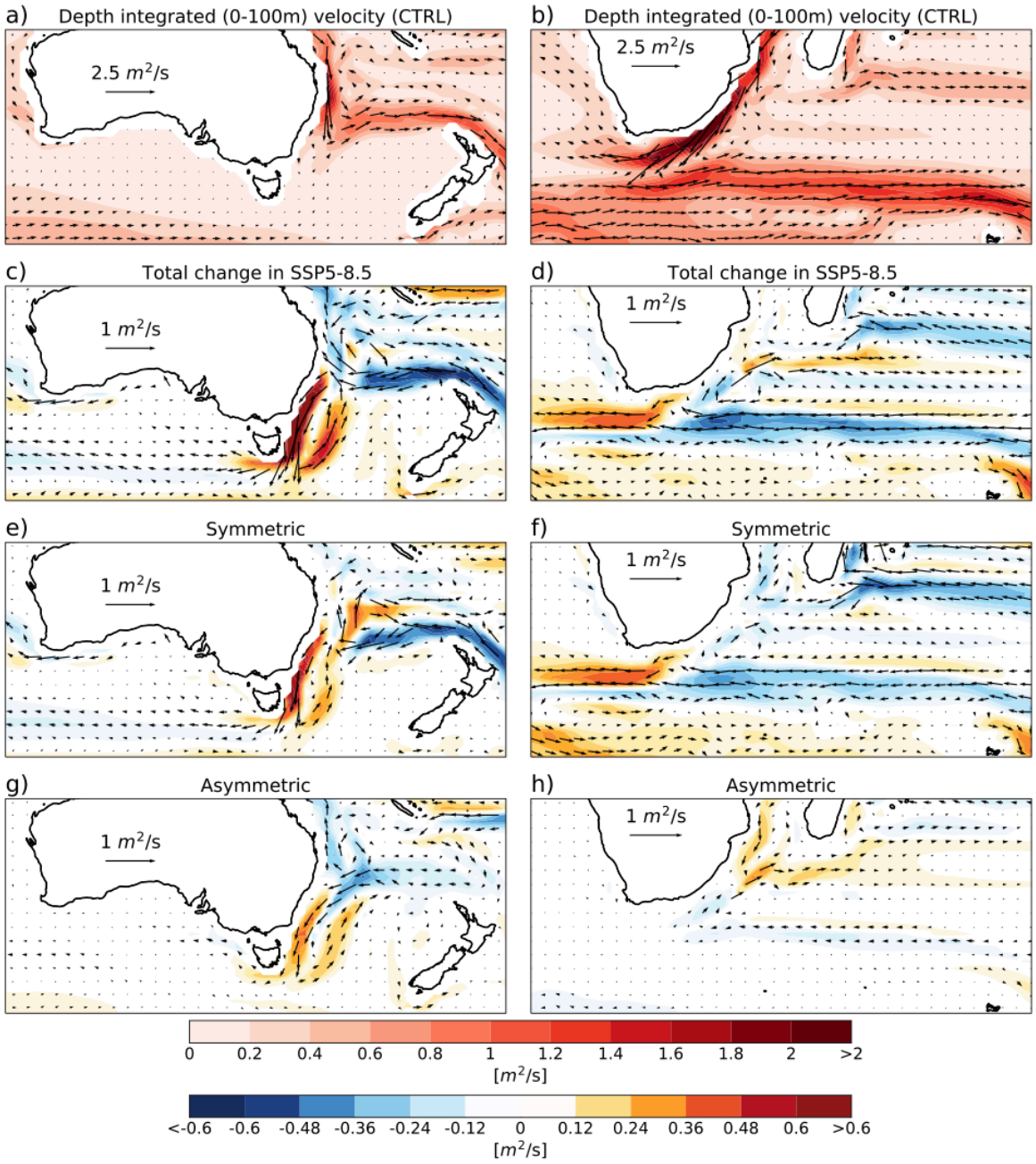

636

637 **Figure 3 |** Depth-integrated ocean currents in the upper 100-m across the different model
638 simulations. Shading shows the depth-integrated current speed and vectors represent the
639 depth-integrated currents. Panels a) and b) respectively represent climatological mean depth
640 (0-100m) integrated East Australia Current (EAC) and the Agulhas Current. Second, third and
641 fourth rows respectively represent the change in the depth (0-100m) integrated currents
642 because of total (*Future* minus *CTRL*), zonally asymmetric (*Symmetric* minus *CTRL*) and zonally
643 asymmetric (*Future* minus *Symmetric*) future atmospheric changes.
644

645

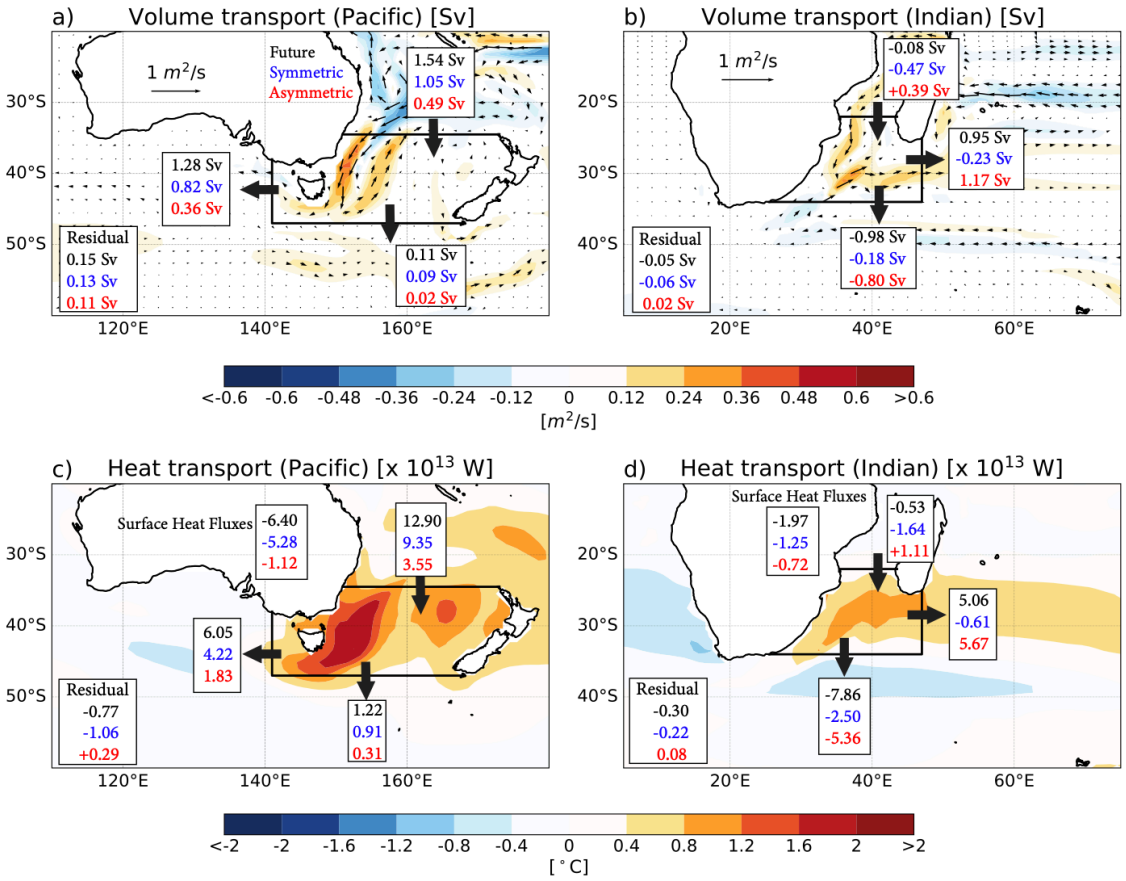

Figure 4 | Volume and heat transport changes (in the upper 100 meters) in the East Australia Current and Agulhas Current regions. Shading in panels a) and b) represents the projected changes in the depth (0 – 100-m) integrated current velocity based on the asymmetric simulation, and numbers represent the change in the volume transport because of total (black), zonally symmetric (blue) and zonally asymmetric (red) atmospheric changes. Shading in panels c) and d) represent the sea surface temperature change because of the zonally asymmetric atmospheric changes and the numbers represent changes in the heat transport because of total (black), zonally symmetric (blue) and zonally asymmetric (red) atmospheric changes.

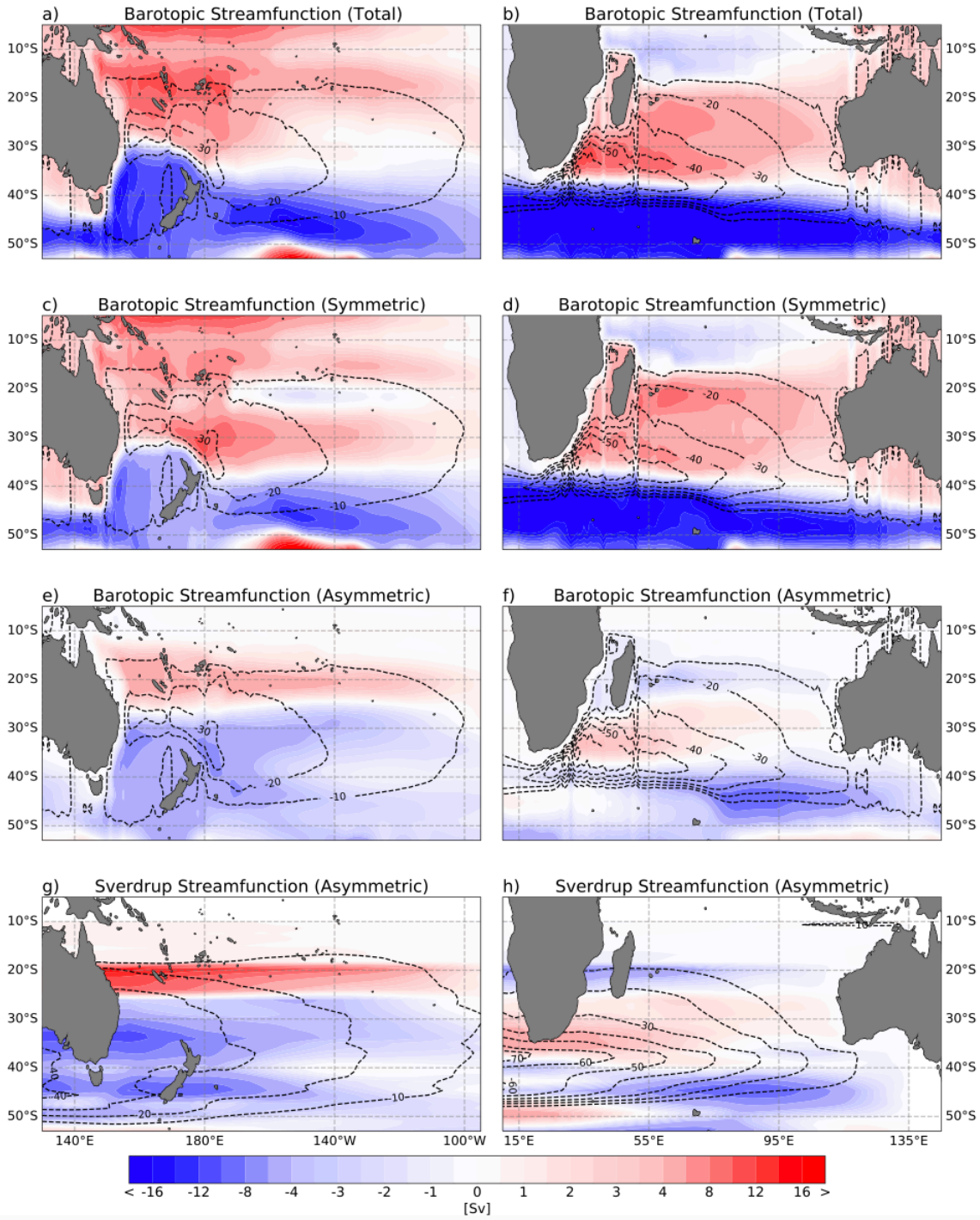

661

662 **Figure 5 |** Changes in the barotropic streamfunction and Sverdrup transport. Shading in the
663 top three rows represent changes in the barotropic streamfunction because of total, zonally
664 symmetric and zonally asymmetric atmospheric changes. Contours in top three rows
665 represent the climatological mean barotropic streamfunction in the *CTRL* simulation. Shading
666 in the bottom row represents change in the Sverdrup streamfunction because of asymmetric
667 atmospheric changes and contours represent the climatological mean Sverdrup
668 streamfunction in the *CTRL* simulation. Sverdrup streamfunction is calculated by basin wide
669 zonal integration of the wind stress curl.